Patterns of synchrony in neuronal networks: the role of synaptic inputs

Igor Belykh and Martin Hasler

Dedicated to Valentin S. Afraimovich on the occasion of his 65th birthday

Abstract We study the role of network architecture and synaptic inputs in the formation of synchronous clusters in synaptically coupled networks of bursting neurons. Through analysis and numerics, we show that the stability of the completely synchronous state, representing the largest cluster, only depends on the number of synaptic inputs each neuron receives, independent from all other details of the network topology. We also give a simple combinatorial algorithm that finds synchronous clusters from the network topology. We demonstrate that networks with a certain degree of internal symmetries are likely to have cluster decompositions with relatively large clusters, leading potentially to cluster synchronization at the mesoscale network level. We address the asymptotic stability of cluster synchronization in excitatory networks of bursting neurons and derive explicit thresholds for the coupling strength that guarantees stable cluster synchronization.

1 Introduction

Brain networks have an hierarchy of different levels, ranging from the microscale via the mesoscale to the macroscale. The microscale is represented by individual neurons and their local synaptic connections. The mesoscale level involves networks of columns and minicolumns, connecting populations of neurons. At the

Igor Belykh
Department of Mathematics and Statistics and Neuroscience Institute, Georgia State University, 30 Pryor Street, Atlanta, GA 30303, USA, e-mail: ibelykh@gsu.edu

Martin Hasler
School of Computer and Communication Sciences, Ecole Polytechnique Fédérale de Lausanne (EPFL), Station 14, 1015 Lausanne, Switzerland e-mail: martin.hasler@epfl.ch

macroscale, large numbers of neuronal populations are arranged into large-scale patterns of anatomical connectivity [1]. The three scale levels determine the functional properties of individual neurons and neuronal networks. As a result, patterns of cooperative neuronal activity also possess multi-level microscopic, mesoscopic, and macroscopic properties. Individual neurons and their dynamics represent the microscale level; cooperative rhythms of neuronal subpopulations define the mesoscale level, and large-scale patterns of activity, such as an average mean field dynamics or synchronization, correspond to the macroscale.

Recently, a great deal of attention has been paid to algebraic, statistical and graph theoretical properties of networks and their relationship to the dynamical properties of the underlying network (see, for example, [2, 3, 4, 5, 6, 7, 8, 9, 10, 11, 12, 13, 14, 15, 16] and the references therein). The most important questions about dynamical networks are those of the interplay between network topology and dynamics: How does network structure affect dynamical properties and information capabilities of networks? Can a dynamical partition of a biological network be inferred from purely topological criteria? Until recently most studies were concerned with the patterns defined by a local microscale network structure or with the macroscopic large-scale patterns of activity such as the mean field dynamics and synchronization. However, the interest has now shifted toward the analysis of cooperative rhythms in subpopulations defined by the mesoscopic modular structure of the network [10]. Different approaches to extracting dynamical properties from topological and modular structures in complex networks of different nature were recently proposed [11, 12, 13].

The simplest macroscopic rhythm in neuronal networks is synchronization when all neurons fire in unison. Synchronized neuronal firing has been suggested as particularly relevant for neuronal signal transmission and coding. While its involvement in cortical processing is somewhat controversial, the presence of synchronization has been shown in special areas such as the olfactory system or the hippocampal region [17]. Model studies of neuronal synchronization can be separated in those where spiking, relaxation oscillator-type models are used, and bursting models are employed [18, 19, 20, 21, 22, 23, 24, 25, 26, 27, 28, 29, 30]. Bursting occurs when neuron activity alternates, on a slow time scale, between a quiescent state and fast repetitive spiking. There has been much work on mechanisms that produce such bursting [31, 32, 33, 34, 35, 36, 37, 38]. In contrast to coupled spiking neurons, whose synchronous dynamics is relatively simple, interacting bursting neurons may exhibit different forms of synchrony; including synchronization of individual spikes, burst synchronization when only the envelopes of the spikes synchronize, and complete synchrony [23, 25, 27]. Typically, burst synchronization arises at a low coupling strength whereas complete synchrony, which involves both burst and spike synchronization regimes, requires a stronger coupling. Models of interacting bursting neurons often use one of two different forms of coupling depending on whether the synapse is electrical or chemical. In the first case, the coupling through gap junctions is linear and directly dependent on the difference of the membrane potentials. In the second case, the coupling is pulsatile and often modeled as a static sigmoidal nonlinear input-output function with a threshold and saturation [53]. The emergence of neuronal synchronization heavily depends on the intrinsic properties

of the individual neurons and the type of synaptic coupling and its network topology [20, 21, 22, 23, 24, 25, 26, 27, 28, 29, 30]. This problem was intensively studied for linearly coupled networks of bursting neurons [20, 25], and more generally, of limit-cycle and chaotic oscillators [4, 5, 6, 7, 8, 9]. In particular, it has been shown that synchrony in such networks strongly depends on the structure and size of the network. In contrast with linearly (electrically) coupled bursting neurons, the stability of synchronization in pulse- (synaptically) coupled networks only depends on the number of signals each neuron receives, independent from all other details of the network topology [27]. In this chapter, we review this result [27] and give additional details of the proof.

Other important examples of cooperative rhythms are clusters of synchrony [39, 40, 41, 43, 44, 45] when the neuronal network splits into subpopulations, called clusters, such that all neurons within one cluster fire in perfect synchrony. The existence of clusters of perfect synchrony is strictly defined by the symmetries of the neuronal network [42, 43, 44, 45] and therefore by a symmetric modular structure of the network. A symmetry of a coupled cell network is defined as a permutation of the cells that preserves all internal dynamics and all couplings. The stability of synchronous clusters in networks of bursting neurons is defined by different factors such as the type of bursting in the individual neuron model and the neuronal connections among and within the clusters.

In this chapter, we also study the emergence of stable synchronous clusters in synaptically coupled networks as a mesoscale phenomenon. We use our recent results [46] to show how to effectively find clusters defined by subnetworks' mesoscopic architecture and symmetries, and derive the conditions on their stability using the Lyapunov function method. We also demonstrate that the same cluster synchronization regimes may have distinct mesoscopic and macroscopic properties. More precisely, we study the existence and stability of synchronous clusters in excitatory networks of Hindmarsh-Rose neurons. We implement the concept of minimal balanced coloring [43, 44, 45] into a combinatorial algorithm for finding synchronous clusters. The core of the minimal balanced coloring concept is that every cluster of synchrony corresponds to a coloring of the network cells in which two cells have the same color if and only if their dynamical variables are equal (completely synchronized). It is important to emphasize that the vertex coloring [43, 44, 45] used in this is *different* from the one defined in graph theory. Graph theory introduces a coloring of a graph as an assignment of colors to the vertices, one color to each vertex, so that adjacent vertices are assigned different colors [49]. However, two adjacent cells from our cluster partition may have the same color as long as their dynamics are described by the same differential equations, up to a permutation of the variables [43].

We use progressive refinement of the coloring map [43, 44, 45] to identify clusters in regular and random networks and come to a natural conclusion that random networks rarely exhibit clusters due to the lack of symmetrical network substructures. We also prove the stability of specific clusters in regular lattices of Hindmarsh-Rose neurons, starting with the proof of complete synchronization in globally and densely synaptically coupled excitatory Hindmarsh-Rose neurons

that exhibit square-wave bursters. To the best of our knowledge, synchronization of *synaptically* coupled square-wave bursters has not previously been proven, and this chapter, following our recent work [46], presents the first proof of this kind. In fact, the well developed theory of weakly coupled oscillators had previously been applied to prove synchronization of elliptic bursters [23] that synchronize at very weak coupling strengths, comparable to a small parameter in the individual neuron system. At the same time, square-wave bursters are notorious for their resistance to synchronization[27] and require a strong synaptic coupling, therefore the reduction to phase models cannot be applied. These two types of bursting were first identified by Rinzel [31, 35]. Square-wave bursting was named after the shape of the voltage trace during a burst which resembles a square wave due to fast transitions between the quiescent state and fast repetitive spiking. Similarly, elliptic bursting received its name due to the shape of the voltage trace that looks like a half-ellipse [35].

The layout of this chapter is as follows. First, in Sec. 2, we introduce the Hindmarsh-Rose neuron model as an individual unit of the network. We analyze its dynamics to find the regions of parameters corresponding to square-wave bursting. Then, we present and discuss the network model. In Sec. 3, we prove that the onset of complete synchrony in a network with any coupling topology admitting complete synchronization is ensured by one single condition, defined by the number of synaptic inputs. To prove the stability of synchronization, we construct a Lyapunov function for the difference variables that allows us to analyze the synchronization properties of the networks without resorting to computer simulation. In Sec. 4, we present the algorithm for finding possible synchronous clusters and apply it to specific networks. We also prove the stability of clusters in regular networks where each cluster of cells is driven by the same driving neurons. Finally, in Sec. 5, a brief discussion of the obtained results is given.

2 The model and problem statement

2.1 Single cell: Hindmarsh-Rose model and its dynamics

We start off with the Hindmarsh-Rose neuron model [47] which represents a class of phenomenological models of spiking and bursting neurons. Without direct relation to concrete physiological mechanisms, these models aim at reproducing the characteristic features of the bursting behavior. To the extent that the assumptions underlying the phenomenological models are sufficiently general, these models may be used to explain generic bifurcation scenarios that can also be observed in the more realistic models.

The Hindmarsh-Rose (HR) model is well-known for its chaotic behavior and different types of bursting [48, 22, 27, 50, 51]. The model takes the form

$$\begin{cases} \dot{x} = y + ax^2 - x^3 - z + I \\ \dot{y} = 1 - dx^2 - y \\ \dot{z} = \mu(b(x - x_0) - z), \end{cases} \tag{1}$$

where x represents the membrane potential, and variables y and z take into account the transport of ions across the membrane through fast and slow ion channels, respectively. Fast variable y describes the rate of change of the fast (e.g., sodium) current. Slow variable z controls the speed of variation of the slow (e.g., potassium) current. This speed is in turn controlled by a small parameter μ. Parameter I describes an external current that enters the neuron. Parameters a and d (b and x_0) describe activation and inactivation of the fast (slow) ion channel. The presence of the small parameter μ in the z-equation makes the system (1) slow-fast, where the (x,y)-equations and z-equation represent fast "spiking" and slow "bursting" subsystems, respectively.

For the sake of simplicity, the original HR model (1) with the redundant set of parameters can be transformed, using the substitution $(y,z) \to (1-y, 1+I+z)$, $d = a+\alpha, c = -1-I-bx_0$, into the form

$$\begin{cases} \dot{x} = ax^2 - x^3 - y - z, \\ \dot{y} = (a+\alpha)x^2 - y, \\ \dot{z} = \mu(bx + c - z). \end{cases} \tag{2}$$

The model (2) can exhibit different types of bursting that have different impacts on the stability of the synchronous solution. Therefore we shall first study the dynamics of the individual model (2) and determine the regions of parameters where square-wave bursting exists. A detailed numerical analysis of bifurcations in the original HR model (1) was recently performed [50, 51].

Readers who are willing to accept the results of this subsection without proof can proceed without loss of continuity to the description of the network model in the next subsection.

We use the standard decomposition of the system (2) into fast and slow subsystems. The fast (x,y)-system has the nullcline $z = f(x) \equiv -\alpha x^2 - x^3$, obtained from solving the system of equations $0 = ax^2 - x^3 - y - z$ and $0 = (a+\alpha)x^2 - y$. The nullcline $z = f(x)$ has two critical points $x_{C1} = -2\alpha/3$ and $x_{C2} = 0$ that correspond to two knees of the graph (see Fig. 1). For simplicity, we shall limit our attention to positive values of parameter α. The generalization to $\alpha < 0$ is straightforward. For $b > \alpha^2/3$ the nullcline of the slow z-equation $z = g(x) \equiv bx + c$ crosses the graph of $f(x)$ at a single point x_e such that the system (2) displays a unique equilibrium point $E(x_e, y_e, z_e)$.

The types of bursting that can exist in the system (2) are defined by the z-parameter sequences of phase portraits of the fast system:

$$\begin{cases} \dot{x} = ax^2 - x^3 - y - z, \\ \dot{y} = (a+\alpha)x^2 - y, \ \ z = \text{const} \end{cases} \tag{3}$$

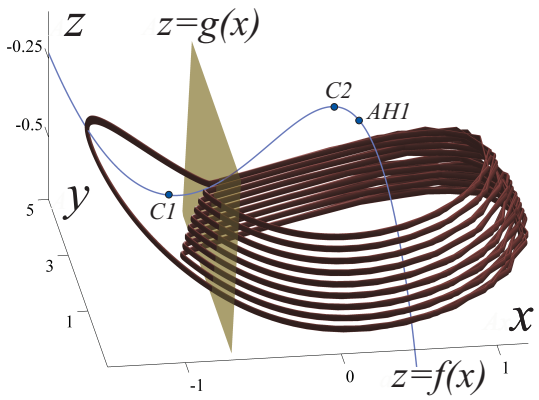

Fig. 1 Square-wave burster of the Hindmarsh-Rose model (2). Parameters $a = 2.8$, $\alpha = 1.6$, $c = 5$, $b = 9$, $\mu = 0.001$. The right stable branch of the fast nullcline $z = f(x)$ contains two points $AH1$ and $AH2$ corresponding to supercritical Andronov-Hopf bifurcations. The second point $AH2$ with $x_{AH2} \approx 1.666$ lies on a much lower part of the nullcline and is not shown.

derived from (2) for $\mu = 0$. This represents the usual adiabatic approach in which the fast system accounts for the fast dynamics (3), and variations of z describe the slow dynamics. Here, the parameters of the fast system a and α determine the types of possible bursting behavior in the full system (2).

I. Fast system. The x-nullcline of the fast system (3) is the curve

$$n_x : \; y = ax^2 - x^3 - z \tag{4}$$

and the y-nullcline is

$$n_y : \; y = (a+\alpha)x^2. \tag{5}$$

Coinciding with the points of intersection between the graphs of (4) and (5), equilibria of the system (3) are determined by the solutions of the equation

$$z = f(x) \equiv -\alpha x^2 - x^3. \tag{6}$$

Hence, for $-\frac{4}{27}\alpha^3 \equiv z_c < z < 0$, $\alpha > 0$ the system (3) has three equilibrium points $N_1(x_1, y_1)$, $O(x_0, y_0)$, and $N_2(x_2, y_2)$, where x_0 and $x_{1,2}$ are the roots of Eq. (6), ordered such that $x_1 < -\frac{2}{3}\alpha < x_0 < 0 < x_2$, and $y_i = (a+\alpha)x_i^2$, $i = 0, 1, 2$. Their stability is defined by the characteristic equation:

$$s^2 - \sigma(x_i)s - f'(x_i) = 0, \; i = 0, 1, 2, \tag{7}$$

where the divergence $\sigma = -(1 - 2ax + 3x^2)$ and the slope $f' = -2\alpha x - 3x^2$. Thus O is a saddle and N_1 and N_2 are stable nodes or foci. The divergence of the two-

dimensional vector field of the fast system (3) changes sign so that

$$\sigma(x) > 0 \text{ for } x_{AH1} < x < x_{AH2}$$
$$\sigma(x) < 0 \text{ for } x < x_{AH1}, \; x > x_{AH2},$$

where the values $x_{AH1,AH2} = (a \mp \sqrt{a^2-3})/3$ correspond to a pair of Andronov-Hopf bifurcations of the equilibrium point N_2 where $\sigma(x_2 = x_{AH1,AH2}) = 0$.

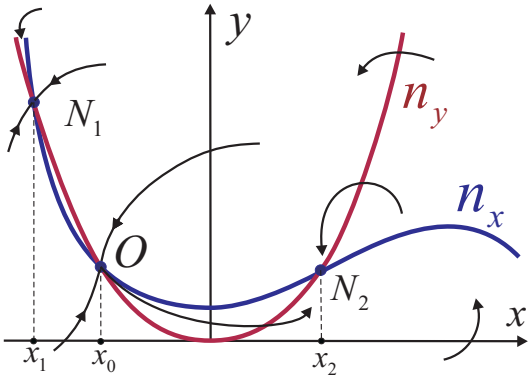

Fig. 2 Nullclines n_x and n_y of the fast system (3). Increasing (decreasing) z shifts the cubic nullcine n_x down (up). For $-\frac{4}{27}\alpha^3 \equiv z_c < z < 0$, there are three equilibrium points N_1, O, and N_2. While z changes, the three points trace out the left, middle, and right branches of the nullcline $z = f(x)$ of the full system (2), respectively (cf. Fig 1). Further increase (decrease) of z makes the saddle O and the equilibrium point N_2 (N_1) disappear.

Using explicit formulas given by Bautin [52], we calculate the first Lyapunov coefficient for the Andronov-Hopf bifurcation of the equilibrium $N_2(x_2, y_2)$ as follows

$$L_1 = -\frac{\pi}{4}|f'(x_2)|^{-3/2}(3+2\alpha a). \tag{8}$$

This value is negative for $\alpha > -3a/2$ which is true for any positive values of a and α. Hence, as z decreases for x_{AH1} (or increases for x_{AH2}), the equilibrium N_2 undergoes a supercritical Andronov-Hopf bifurcation such that a unique stable cycle appears softly from N_2.

Using the nullclines n_x and n_y together with the flows shown in Fig. 2, we can deduce the following general properties of the vector field.

Property 2.1. All trajectories of the system (3) leave the region $\{y < 0\}$.

Property 2.2. The system has the absorbing domain $Ab = \{|x| < |x_p|,\ 0 \le y \le y_p\}$, where $y_p = (a+\alpha)x_p^2$ and x_p is either the largest root of equation $x^3 - ax^2 + z = 0$, or the coordinate of the equilibrium point N_1.

Property 2.3. For $x_0 < x_{AH1}$ the limit cycles of the system (3) can only encircle the equilibrium point N_2, i.e., the fast HR model can not produce cycles encircling only equilibrium point N_1, nor can it have cycles enclosing all three equilibrium points.

This property follows from the orientation of the vector field as cycles encircling either the equilibrium N_1, or all three equilibria would have to wind against the vector field (cf. the vector field around N_1).

Property 2.4. A homoclinic orbit of O may exist only in the region $x > x_0$ as it is constrained by the vector field, similar to Property 2.3.

II. Square-wave bursting. According to the above analysis, the behavior of the fast system is essentially different for $a \leq \sqrt{3}$ and $a > \sqrt{3}$.

Region 1: $a \leq \sqrt{3}$. As the divergence $\sigma(x) \leq 0$ everywhere, the fast system has no cycles. The equilibrium points N_1 and N_2 are stable, and the stable manifold of the saddle O (when it exists) divides the (x,y) plane into the basins of attraction of N_1 and N_2. As a result, the dynamics of the full system (2) is qualitatively similar to that of the FitzHugh-Nagumo system. That is, with a proper location of the slow nullcline $z = g(x)$, intersecting the middle branch of the fast nullcline $z = f(x)$, the system has an unstable equilibrium encircled by a stable relaxation oscillator-type cycle defining the simplest form of bursting.

Region 2: $a > \sqrt{3}$. The equilibrium point N_2 of the fast system undergoes a supercritical Andronov-Hopf bifurcation for $x_2 = x_{AH1}$, and the homoclinic orbit of the saddle O is always stable (the corresponding saddle value is negative). In this case, the dynamics of the fast system is as follows. For $z < z_{AH2}$ the equilibrium point N_2 is globally stable. For $z_{AH2} < z < z_c$ there exists a stable cycle encircling the unstable equilibrium point N_2. For $z_c < z < z_h$ the unstable manifold W^u of the saddle O consists of two separatrices so that one of them approaches the stable cycle and the other is attracted by the stable equilibrium point N_1. At $z = z_h$ the stable cycle turns into a homoclinic loop, and for $z > z_h$ the separatrices of O change their arrangement so that all trajectories of the system (3), except the stable manifold of O and the unstable equilibrium point N_2, approach the stable equilibrium N_1. The result is a spiking manifold that is composed of the limit cycles of the fast system. Its upper edge is defined by the homoclinic bifurcation at $z = z_h$. Depending on the location of the slow nullcline $z = g(x)$, intersecting the middle branch of the fast nullcline $f(x)$, the full system can generate either square-wave bursting (see. Fig. 1) or tonic spiking. In the Izhikevich classification, [35] this scenario describes the mechanism of formation of the fold/homoclinic burster which is referred to as being square-wave bursting due to the voltage amplitude profile [35]. Bifurcations and complicated sets associated with the transition from tonic spiking into square-wave bursting in various neuronal models have been extensively studied [32, 34, 36, 37, 38].

In the following, we will concentrate on the parameters from region 2 where the individual HR model (2) can generate square-wave bursting. Hereafter, the parameters are chosen and fixed as follows: $a = 2.8$, $\alpha = 1.6$, $c = 5$, $b = 9$, $\mu = 0.001$.

2.2 Network of synaptically coupled neurons

Consider now a network of n synaptically coupled HR models (2). The equations of motion read:

$$\begin{cases} \dot{x}_i = ax_i^2 - x_i^3 - y_i - z_i + g_{\rm s}(V_{\rm s} - x_i) \sum\limits_{j=1}^{n} c_{ij}\Gamma(x_j), \\ \dot{y}_i = (a+\alpha)x_i^2 - y_i, \\ \dot{z}_i = \mu(bx_i + c - z_i),\ i,j = \overline{1,n}. \end{cases} \tag{9}$$

Here, each neuron is represented by the HR model (2), and the neurons are identical. The synapses are fast and instantaneous, i.e. time delays and internal synaptic variables are ignored. The parameter $g_{\rm s}$ is the synaptic coupling strength. The reversal potential $V_{\rm s} > x_i(t)$ for all x_i and all times t, i.e. the synapse is excitatory. The synaptic coupling function is modeled by the sigmoidal nonlinear input-output function $\Gamma(x_j) = 1/[1+\exp\{-\lambda(x_j - \Theta_{\rm s})\}]$. This oft-used coupling form was called fast threshold modulation by Somers and Kopell [53]. The threshold $\Theta_{\rm s}$ is chosen such that every spike in the single neuron burst can reach the threshold (see Fig. 3). Hereafter, $\Theta_{\rm s} = -0.25$ and $V_{\rm s} = 2$.

In (9), $\mathbf{C} = (c_{ij})$ is the $n \times n$ connectivity matrix: $c_{ij} = 1$ if neuron i receives synaptic input from neuron j, $c_{ij} = 0$ otherwise, and $c_{ii} = 0$. Matrix $\mathbf{C}$ can be asymmetric such that both mutual and unidirectional couplings are allowed. We require the connectivity matrix $\mathbf{C}$ to have at least some rows with equal row-sums $k_i = \sum\limits_{j=1}^{n} c_{ij}$, $i = 1,...,n$. This requirement is a necessary condition for the existence of synchronous clusters of neurons whose states are equal. The existence of clusters yields a decomposition of the network (9) into the disjoint subsets of vertices (neurons) $V = V_1 \cup ... \cup V_d$, $V_\gamma \cap V_\nu = \emptyset$ given by the equalities of the neuron states. If the decomposition is flow-invariant with respect to the vector field of the system (9), then the corresponding linear subspace $M(d)$ is invariant and defines d synchronous clusters.

3 Complete synchronization in the network

The Section reports a surprising find regarding the synchronization of pulse-coupled networks of bursting neurons [27]. We study the stability of full complete synchronization in networks of HR neurons (9) where each neuron receives signals from k others, where k is uniform for all neurons. In the following, we demonstrate that all that matters for the onset of complete synchrony is the number of signals, k, received by each neuron. This is independent of all other details of the network structure. More precisely, the synchronization threshold is inversely proportional to the number of incoming signals k. This criterion applies to a neuronal network with *any* coupling topology admitting complete synchrony.

For this property to be true, we require matrix $\mathbf{C}$ to have equal row-sums $k = \sum\limits_{j=1}^{n} c_{ij}$, $i = 1,...,n$. This requirement is a necessary condition for the existence of the synchronous solution, namely the invariance of hyperplane $M(1) = \{\xi_1(t) = \xi_2(t) = ... = \xi_n(t)\}$, $\xi_i = (x_i, y_i, z_i)$, $i = \overline{1,n}$. In fact, the equal row-sum property implies a

network where each cell has the same number k of inputs from other neurons. Note that this k-row sum matrix $\mathbf{C}$ can be asymmetric such that directed networks with the same node in-degree k are also allowed.

Synchronous behavior on the manifold $M(1)$ is generated by the self-coupled system:

$$\begin{cases} \dot{x} = ax^2 - x^3 - y - z + kg_{\rm s}(V_{\rm s} - x)\Gamma(x), \\ \dot{y} = (a+\alpha)x^2 - y, \\ \dot{z} = \mu(bx + c - z). \end{cases} \tag{10}$$

Consequently, the synchronous behavior differs from the behavior of the uncoupled neuron and depends on the coupling strength $g_{\rm s}$. The analysis of the slow-fast individual HR system, performed in Sec. 2, carries over to the self-coupled system. The main difference is that the fast subsystem of the self-coupled system undergoes Andronov-Hopf bifurcations at new points $x^{\rm self}_{AH1,AH2} = (a \mp \sqrt{a^2 - 3(kg_s + 1)})/3$. Hence, increasing the coupling $g_{\rm s}$ makes the points x_{AH1} and x_{AH2} move towards each other along the fast nullcline $f(x)$ of the self-coupled system (cf. Figs. 3 and 1). Hence, for $kg_{\rm s} = a^2/3 - 1$ the two points merge together such that for $kg_{\rm s} > a^2/3 - 1$ there is no oscillatory (spiking) dynamics on the right branch of the fast nullcline as the Andronov-Hopf points have disappeared. Thus, there is no square bursting for $kg_{\rm s} > a^2/3 - 1$, and the synchronous dynamics defined by the self-coupled system (10) is of relaxation oscillator-type.

We begin by deriving the variational equations for the transverse stability of the synchronization manifold $M(1)$.

Adding and subtracting an additional term $g_{\rm s}(V_{\rm s} - x_i)\sum_{j=1}^{n} c_{ij}\Gamma(x_i) = kg_{\rm s}(V_{\rm s} - x_i)\Gamma(x_i)$ from the x-equation of system (9), yields

$$\begin{cases} \dot{x}_i = ax_i^2 - x_i^3 - y_i - z_i + kg_{\rm s}(V_{\rm s} - x_i)\Gamma(x_i) + g_{\rm s}(V_{\rm s} - x_i)\sum_{j=1}^{n} c_{ij}\left(\Gamma(x_j) - \Gamma(x_i)\right), \\ \dot{y}_i = (a+\alpha)x_i^2 - y_i, \\ \dot{z}_i = \mu(bx_i + c - z_i),\ i,j = \overline{1,n}. \end{cases} \tag{11}$$

Introducing the differences between the neural oscillator coordinates $X_{12} = x_2 - x_1$, $Y_{12} = y_2 - y_1$, $Z_{12} = z_2 - z_1$ in the limit when these differences are infinitesimal, we derive the stability equations for the transverse perturbations to the synchronization manifold $M(1)$[27]:

$$\begin{cases} \dot{X}_{ij} = (2ax - 3x^2)X_{ij} - Y_{ij} - Z_{ij} - kg_{\rm s}\Gamma(x)X_{ij} + \\ \qquad + g_{\rm s}(V_{\rm s} - x)\Gamma_x'(x)\left(kX_{ij} + \sum_{h=1}^{n}\{c_{jh}X_{jh} - c_{ih}X_{ih}\}\right), \\ \dot{Y}_{ij} = 2(a+\alpha)xX_{ij} - Y_{ij}, \\ \dot{Z}_{ij} = \mu(bX_{ij} - Z_{ij}). \end{cases} \tag{12}$$

The derivatives are calculated at the point $X_{ij} = 0, Y_{ij} = 0, Z_{ij} = 0$, and $\{x(t), y(t), z(t)\}$ corresponds to the synchronous bursting solution defined via system (10). The first coupling term $S_1 = -kg_{\rm s}\Gamma(x)X_{ij}$ accounts for the number of inputs k. At the

same time, the contribution of the second coupling term $S_2 = g_s(V_s - x)\Gamma_x'(x)(\cdot)$ depends on the coupling configuration. Note that the term $\sum_{h=1}^{n}\{c_{jh}\xi_{jh} - c_{ih}\xi_{ih}\}$ is the same as for linear coupling [6]. In terms of the original variables x_i, the corresponding coupling matrix $\mathbf{G} = \mathbf{C} - k\mathbf{I}$ is the Laplacian of the connected graph, except for a sign change. It is well known that $\mathbf{G}$ has one zero eigenvalue γ_1 and all other eigenvalues have non-positive real parts. If the coupling is mutual, $\mathbf{G}$ is symmetric and all eigenvalues are real. For simplicity, suppose that the eigenvalue γ_2 with the largest real part is simple. Then, applying the linear transformation that diagonalizes $\mathbf{G}$ to Eq. (12), we obtain the stability equation for the most unstable transverse mode:

$$\begin{aligned} \dot{X} &= (2ax - 3x^2)X - Y - Z - \Omega(x)Z, \\ \dot{Y} &= 2(a+\alpha)xX - Y, \\ \dot{\zeta} &= \mu(bX - Z), \end{aligned} \tag{13}$$

where $\Omega(x) = kg_s\Gamma(x) - g_s(V_s - x)\Gamma_x'(x)(k+\gamma_2)$. System (13) is an analog of the Master Stability function [6] for synaptically coupled networks (9). If γ_2 is not simple, then we can write similar equations to system (13) for the vectors spanning the corresponding blocks in the Jordan normal form of $\mathbf{G}$. The stability discussion, however, is essentially the same. Consider now its application to basic network configurations.

3.1 Globally coupled networks

In this case, the second largest eigenvalue $\gamma_2 = -n$ and $k = n-1$. Consequently, the function $\Omega(x)$ becomes

$$\Omega(x) = kg_s\Gamma(x) + g_s(V_s - x)\Gamma_x'(x) = \frac{kg_s}{1+\exp\{-\lambda(x-\Theta_s)\}} + g_s(V_s - x)\frac{\lambda\exp\{-\lambda(x-\Theta_s)\}}{(1+\exp\{-\lambda(x-\Theta_s)\})^2} \tag{14}$$

The function $\Gamma(x)$ together with its derivative $\Gamma_x'(x)$ is non-negative, and $(V_s - x)$ is always positive (the synapses are excitatory). Therefore $\Omega(x)$ is always non-negative and the coupling term $-\Omega(x)X$ aims at stabilizing the zero equilibrium of system (13); corresponding to the synchronous solution. The function $\Omega(x)$ strongly depends on whether the membrane potential $x(t)$ exceeds the threshold Θ_s or not (see Fig. 3). In fact, for a sufficiently large λ ensuring a bell-shape graph $\Omega(x)$ [46], kg_s is a lower bound of $\Omega(x)$ in the region $x(t) > \Theta_s$ and strongly contributes to the stability. At the same time, when $x(t)$ is below Θ_s, the first term in $\Omega(x)$ rapidly decreases to zero, and the second coupling term becomes decisive in a small region close to $x = \Theta_s$. This region is defined by the parameter λ. For our results concerning the stability of synchronization, it is also necessary to assume that λ is only moderately large. Our stability approach does not carry over to the case where the function $\Gamma(x)$ is approaching the Heaviside function when λ approaches infinity. In

fact, the bounds of Theorem 1 on the sufficient coupling strength become too conservative when λ approaches infinity. At the same time, to prove synchronization of bursters, we do not require μ to be a singular perturbation parameter. Applying the Lyapunov function method to the stability of system (13) with the function (14), we prove the following theorem that synchronization in the globally coupled network can be made stable, provided that the coupling g_s is sufficiently strong.

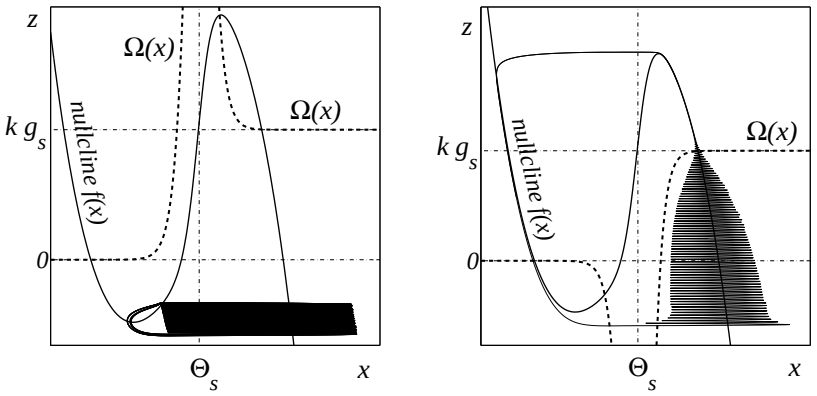

Fig. 3 The function $\Omega(x)$ and the corresponding synchronous bursting. Globally coupled HR neurons ($k = n-1$, $\lambda = 10$) (left). Ring of locally coupled HR neurons ($k = 2$, $\lambda = 10$) (right).

Theorem 1. *Complete synchronization in the globally coupled network (9) with the number of synaptic inputs $k = n-1$ is locally stable if the coupling g_s exceeds the critical value*

$$g_s^* = \max\{D_1, D_2, D_3\}, \text{ where} \tag{15}$$

$$\begin{aligned} &D_1 = \tfrac{a^2}{3k}, \ D_2 = \tfrac{(a-\alpha)^2}{4k(3-\beta(a+\alpha)^2)} + \tfrac{1}{4k\beta}, \ \beta < 3/(a+\alpha)^2, \\ &D_3 = \tfrac{p(1+e^{-\lambda(b-\Theta_s)})^2}{\beta[k(1+e^{-\lambda(b-\Theta_s)})+(V_s-b)\lambda e^{-\lambda(b-\Theta_s)}]}, \\ &b = \tfrac{(a-\alpha)-\sqrt{(a-\alpha)^2+(3/\beta-(a+\alpha)^2)}}{2(3-\beta(a+\alpha)^2)} \\ &\text{for } a \geq \alpha: \ p = \tfrac{1}{4} \text{ and } \quad \text{for } a < \alpha: \ p = \tfrac{1}{4} + \tfrac{\beta(a-\alpha)^2}{4(3-\beta(a+\alpha)^2)}. \end{aligned} \tag{16}$$

Proof. Consider the Lyapunov function

$$\Phi = X^2/2 + \beta Y^2/2 + \frac{1}{2\mu b} Z^2, \tag{17}$$

where β is a positive auxiliary parameter to be defined.

The derivative of the Lyapunov function (17) with respect to the variational equations (13)-(14) is calculated as follows

$$\dot{\Phi} = -\left\{AX^2 - BXY + \beta Y^2 + Z^2/b\right\}, \tag{18}$$

where $A = [3x^2 - 2ax + \Omega(x)]$ and $B = (2\beta(a+\alpha)x - 1)$.

Our goal is to prove the negative definiteness of the quadratic form $\dot{\Phi}$ and to obtain conditions under which solutions of the variational equation (13)-(14) converge to 0 as $t \to \infty$, and its trivial equilibrium, corresponding to the synchronization manifold of system (9), is locally asymptotically stable.

The quadratic form $\dot{\Phi}$ is negative definite as long as the quadratic form

$$W = -\left\{AX^2 - BXY + \beta Y^2\right\}$$

is negative.

Applying Sylvester's criterion for the negative definiteness of the quadratic form W, we obtain the following two conditions.

Condition I: $A > 0$.

Part 1. If $x \geq \Theta_s$ then the condition $A > 0$ is true if $3x^2 - 2ax + kg_s > 0$. Here, we have taken the lowest bound (kg_s) of the function $\Omega(x)$ in the region $x \geq \Theta_s$ (cf. Fig. 3). The roots of the quadratic equation are $x^r_{1,2} = \left(a \pm \sqrt{a^2 - 3kg_s}\right)/3$. Therefore, this equation has no solutions for

$$g_s > \frac{a^2}{3k}. \tag{19}$$

Part 2. For $x \leq \Theta_s$ and for the given $\Theta_s = -0.25$, A is always positive.

Condition II. The second condition of Sylvester's criterion is $\beta A - B^2/4 > 0$. This leads to the inequality

$$Q(x) \equiv \varphi(x) + \Omega(x) > 0, \text{ where} \tag{20}$$

$\varphi(x) = \beta(3 - \beta(a+\alpha)^2)x^2 - \beta(a-\alpha)x - 1/4$.

The function $\Omega(x)$ is non-negative for any $x(t)$ while the parabola $\varphi(x)$ can be negative in some interval of $x(t)$. To satisfy the condition (20), we should increase the values of the function Ω by increasing the coupling g_s such that the superposition of the two functions becomes positive.

First of all, we require $(3 - \beta(a+\alpha)^2) > 0$ to keep the parabola $\varphi(x)$ concave up. This constrains the choice of the auxiliary parameter β. As the region of parameters where square-wave bursters can exist in the individual HR model (2) is defined by the condition $\{a \geq \sqrt{3}\}$ (Region 2), we have to choose $\beta < 1$ for synchronization of square-wave bursters.

The roots of the parabola $\varphi(x)$ are

$$x^r_{1,2} = \frac{(a-\alpha) \pm \sqrt{(a-\alpha)^2 + (3/\beta - (a+\alpha)^2)}}{2(3 - \beta(a+\alpha)^2)}$$

such that the function $\varphi(x)$ is positive outside the region $[x^r_1, x^r_2]$.

We derive the conditions for Eq. (20) in two steps, considering two parts of the bursting solution (10): $x \geq \Theta_s$ and $x < \Theta_s$.

Part 1. $x \geq \Theta_s$.

As before, we take the lowest bound (kg_s) of $\Omega(x)$ in the region $x \geq \Theta_s$ such that the condition (20) becomes

$$(3-\beta(a+\alpha)^2)x^2-(a-\alpha)x-\frac{1}{4\beta}+kg_s>0.$$

This is true under the conditions

$$g_s > g_s^* = [\tfrac{(a-\alpha)^2}{4k(3-\beta(a+\alpha)^2)}+\tfrac{1}{4k\beta}], \quad \beta < 3/(a+\alpha)^2 \tag{21}$$

Part 2. $x < \Theta_s$.

The minimum of the parabola $\varphi(x)$ is reached at $x^* = \frac{a-\alpha}{2(3-\beta(a+\alpha)^2)}$. If $a < \alpha$ then x^* lies in the region $x < \Theta_s < 0$ and the minimum of the function φ is $\varphi(x^*) \equiv -m = -1/4 - \frac{\beta(a-\alpha)^2}{4(3-\beta(a+\alpha)^2)}$. If $a > \alpha$ then the minimum value of $\varphi(x)$ in the region $x < \Theta_s < 0$ becomes

$$\varphi(\Theta_s) = \beta(3-\beta(a+\alpha)^2)\Theta_s^2+\beta(a-\alpha)|\Theta_s|-1/4.$$

Therefore we take $\varphi(\Theta_s) = -1/4$ as the ultimate bound for the case $a > \alpha$.

To compensate these negative mimimum values of $\varphi(x)$, we should make the coupling strength g_s sufficiently strong such that the minimum value of the positive function $\beta\Omega(x)$ in the interval $[x_2^r, \Theta_s]$ is greater than $-m$ and $-1/4$ for $a < \alpha$ and $a > \alpha$, respectively.

The function $\Omega(x)$ reaches its minimum at the left endpoint of the interval $[x_2^r, \Theta_s]$

$$b = x_2^r = \frac{(a-\alpha)-\sqrt{(a-\alpha)^2+(3/\beta-(a+\alpha)^2)}}{2(3-\beta(a+\alpha)^2)}.$$

Hence, the stability condition (20) for the region $x < \Theta_s$ becomes

$$\begin{aligned} &g_s > g_s^* = \tfrac{p(1+e^{-\lambda(b-\Theta_s)})^2}{\beta[k(1+e^{-\lambda(b-\Theta_s)})+(V_s-b)\lambda e^{-\lambda(b-\Theta_s)}]}, \\ &p = m \text{ for } a < \alpha; \ p = 1/4 \text{ for } a > \alpha; \ \beta < 3/(a+\alpha)^2. \end{aligned} \tag{22}$$

Combining the conditions (19), (21), and (22), we obtain an upper bound for the negative definiteness of the quadratic form $\dot{\Phi}$ and come to the conditions of the Theorem. □

Remark 1. Condition for D_3 in Theorem 1 gives a large overestimate. This is due to the simplifications made in estimating the positiveness of the function $Q(x)$. To obtain a tighter bound for the coupling threshold g_s^* that would replace the constant D_3, we should resolve the transcendental equation (20) with respect to g_s

$$Q(x) = \beta(3-\beta(a+\alpha)^2)x^2 - \beta(a-\alpha)x - 1/4 + \beta\frac{g_s^*}{1+e^{-\lambda(U-\Theta_s)}} + \\ +\beta k g_s^*(V_s-U)\frac{\lambda e^{-\lambda(U-\Theta_s)}}{(1+e^{-\lambda(U-\Theta_s)})^2} = 0, \tag{23}$$

taking into account the condition $\beta < 3/(a+\alpha)^2$. We shall find the solution of Eq. (23) only in the region $x < \Theta_s$. In fact, the bound D_2 (cf. Theorem 1) for the region $x > \Theta_s$ is close to an optimum.

One can see that the equation (23) has a unique solution with respect to g_s^* in the region $x < \Theta_s$ that can be found numerically. Therefore, we can formally substitute D_3 in Theorem 4.1 by $D_3^{\text{new}} = g_s^{\text{cr}}$, where g_s^{cr} is the solution of Eq. (23) in the region $x < \Theta_s$. Note that for a relatively sharp saturating coupling function (λ is relatively large), the constant D_3 (or the corresponding D_3^{new}) often dominates over D_1 and D_2.

Remark 2. The analysis shows that the major part of the quiescent (slow) mode of the synchronous solution, where the contribution of $\Omega(x)$ is negligible, lies in a stable zone $x < x_1^r$, where function $\varphi(x)$ is positive. Here, the derivative of the Lyapunov function is always negative, i.e. where the solutions of the individual systems converge to each other. On the other hand, the part of the bursting solution that is the most difficult to synchronize, favorably lies in the region $x(t) \geq \Theta_s$, where the contribution of $\Omega(x) = kg_s$ is strong and depends on k. This property will re-appear for the densely and sparsely networks later in the text.

Theorem 1 guarantees the stability of the synchronized solution, where the solution could be an equilibrium, a limit cycle defining periodic bursting, or a chaotic attractor corresponding to a chaotic bursting rhythm. The type of the synchronous dynamics is determined by the self-coupled system (10), possessing the additional coupling-dependent term. Let us calculate the synchronization threshold g_s^* (15) with D_3^{new} for the simplest two-neuron globally coupled network (9) with $k = 1$ and parameters of the individual HR model (2) given in Fig. 1. The auxiliary parameter β is chosen from the condition $\beta < 3/(a+\alpha)^2$ and set equal to 0.14. Therefore, the upper synchronization bounds D_1 and D_2 calculated from (15), become $D_1 = 2.61$ and $D_2 = 2.7$. The bound D_3^{new} that we calculate from the transcendental equation ($Q(x) = 0$) (23) becomes $g_s = D_3^{\text{new}} = 2.94$. Therefore, the final upper bound is $g_s^* = \max\{D_1, D_2, D_3^{\text{new}}\} = 2.94$. Numerical simulation shows that complete synchronization arises in the system (9) at a relatively strong coupling $g_s^* = 1.28$. Our bound $g_s^* = 2.94$ clearly gives an overestimate as it comes from sufficient conditions of stability, however it is consistent with non-trivial synchronous behavior.

3.2 Densely coupled networks

We define a densely coupled coupled network (9) as a network (9) for which the eigenvalue γ_2 of $\mathbf{G}$ is close to $-k$. For example, for a ring of $2K$-nearest neighbor mutually coupled neurons, $\gamma_2 = -4\sum_{l=1}^{K}\sin^2\frac{l\pi}{n}$ [54] with $n = 10$, $K = 4$, and $k =$

$2K = 8$, we obtain $\gamma_2 \approx -7.976$. Consequently, the function $\Omega(x)$ becomes close to $kg_s\Gamma(x)$. Therefore, if k is sufficiently large, the bound for the synchronization threshold is close to that for globally coupled networks. In particular, the following theorem holds.

Theorem 2. *An upper bound for the coupling threshold that guarantees local stability of synchronization in the (dense) network (9) with the eigenvalue γ_2 of* **G** *smaller than or equal to $-k$ is*

$$g_s^* = \max\{D_1, D_2, D_3^{\text{dense}}\}, \text{ where} \tag{24}$$

constants D_1 and D_2 are given in the condition (15) of Theorem 1. Here, the new constant $D_3^{\text{dense}} = \frac{p(1+e^{-\lambda(b-\Theta_s)})^2}{\beta[k(1+e^{-\lambda(b-\Theta_s)})-(k+\gamma_2)(V_s-b)\lambda e^{-\lambda(b-\Theta_s)}]}$, and parameters p, b, and β are given in (15).

Proof. The proof is identical to that of Theorem 1 except for the change of function $\Omega^{\text{dense}}(x) = kg_s\Gamma(x) - (k+\gamma_2)g_s(V_s - x)\Gamma_x'(x)(k+\gamma_2)$. □

Remark 3. Note that the second term $-(k+\gamma_2)g_s(V_s-x)\Gamma_x'(x)$ in the denominator of D_3^{dense} is positive as long as $-\gamma_2 > k$ and therefore contributes to lowering the coupling threshold g_s^*. This term, however, is small compared to the first term in the denominator that is decisive for the stability and directly proportional to the number of synaptic inputs k. Consequently, the coupling threshold g_s^* is inversely proportional to k, as in the globally coupled networks.

3.3 Intermediately and sparsely coupled networks

When the number of links between the neurons in a network is small, the eigenvalue γ_2 is also small such that the second term in $\Omega(x)$, $-g_s(k+\gamma_2)(V_s-x)\Gamma_x'(x)$ no longer favors the stability. Consequently, the function $\Omega(x)$ takes negative values in the region close to the threshold Θ_s and defines the instability zone, where the coupling desynchronizes the neurons. At the same time, the stability zone is defined by the first term in Ω, $kg_s\Gamma(x)$, which is bounded from below by kg_s in the region $x(t) \geq \Theta_s$ (cf. Fig. 3 (right)). Strictly speaking, while we are no longer able to prove that the systems synchronize within the framework of the Lyapunov function method, the slow-fast structure of the self-coupled system (10), defining the synchronous solution, yields the following. The excitatory coupling raises the x-nullcline $f(x) = -\alpha x^2 - x^3 - kg_s(x-V_s)\Gamma(x)$ of system (10) such that the right-branch attractor corresponding to spiking gradually moves to the right from the threshold $x = \Theta_s$. Finally, it leaves the zone where $\Omega(x)$ is negative (cf. Fig. 3 (right)), provided g_s is large enough. Note that the raising of the nullcline and the shift of the attractor are also governed by kg_s (cf. Eq. (10)). In the singular perturbation limit ($\mu \to 0$), the synchronous trajectory traverses the instability region via fast jumps from the quiescent mode to repetitive spiking, and spends almost all its

time in the stability regions. As in the case of the global coupling, the first stability zone corresponding to a major part of the slow motion along the left branch of $f(x)$ is always stable, whereas the stability of the second zone corresponding to spiking is defined by kg_s. Hence, once again we see that the synchronization threshold in sparsely and intermediately connected networks is also inversely proportional to k.

3.4 Arbitrary network topology: what matters for synchronization

Collecting all the considered coupling topologies and the conditions of Theorems 1 and 2, we come to the following assertion [27].
Statement 1. *The synchronization threshold estimate*

$$g_s^* = g_s^{(n=2)}/k, \tag{25}$$

is valid for the networks (9) with any coupling configuration (whether global or local, regular or random, mutual or unidirectional) under the constraint that each neuron has the same number of inputs k. In (25), $g_s^{(n=2)}$ is a constant corresponding to the synchronization coupling threshold between two mutually coupled HR neurons ($k = 1$).

Remark 4. The constant $g_s^{(n=2)}$ comes from sufficient conditions and therefore gives an overestimate for the real coupling strength that leads to complete synchronization of two HR neurons: 2.94 predicted versus 1.285 actual for the above mentioned parameters and $\lambda = 10$. However, using the numerically obtained $g_s^{(n=2)}$, we can predict the threshold g_s^*, for any k, from (25), as shown in the numerical examples below.

Remark 5. The synchronization threshold in locally synaptically coupled networks is constant; $g_s^* = g_s^{(n=2)}/2$ for mutually nearest-neighbor coupled neurons, and does not depend on the number of neurons n. This is in sharp contrast with linearly coupled networks where the coupling required for stable synchronization has a quadratic dependence on n [9].

In support of this claim, we determine numerically the threshold for complete synchronization as a function of k for various coupling configurations (local, intermediate and global), and compare it to the value predicted by Eq. (25). For $g_s^{(n=2)}$, the value from simulation of two mutually coupled HR neurons was used. This value is $g_s^{(n=2)} = 1.285$ for $\lambda = 10$ and $g_s^{(n=2)} = 1.139$ for $\lambda = 50$. It can be seen from Fig. 4 that the deviation of the data from the fitted curve is very small indeed. Note that even for large λ, when the synaptic function $\Gamma(x_i)$ approaches the Heaviside function, the estimate (25) gives an excellent numerical prediction (cf. Fig. 4 (right)).

To illustrate the power of condition (25) even further we have simulated -in addition to the regular, mutually coupled networks from Fig. 4- a series of randomly

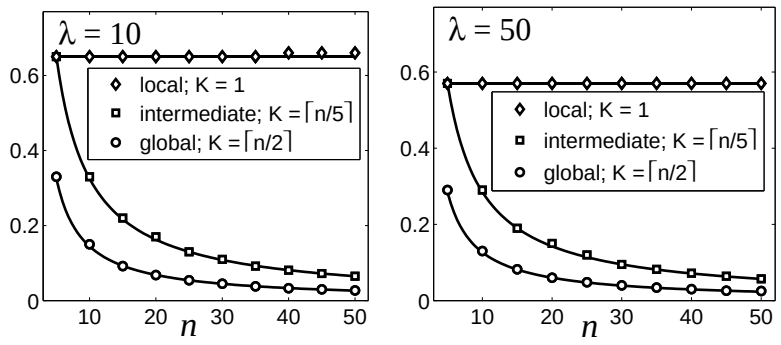

Fig. 4 Synchronization thresholds g_s^* in a ring of $2K$-nearest neighbor coupled HR neurons as functions of n for various coupling configurations (different K). Markers: Simulation results. Solid line: Prediction of Eq. (25).

generated *unidirectionally* coupled networks of HR neurons with uniform number of synapses as those shown in Fig. 5. For all simulated networks, numerical results are nearly identical to the analytical predictions of Eq. (25).

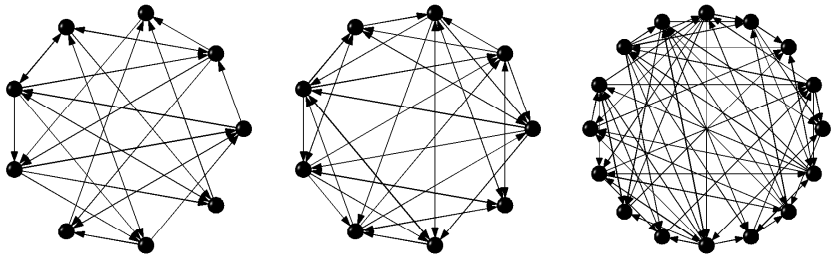

Fig. 5 Ten networks of each type, (left): $n = 9$, $k = 3$; (middle): $n = 9$, $k = 4$; (right): $n = 16$, $k = 4$ were generated randomly. The synchronization threshold for networks of type (a): $g_s^* = 0.429$ for $\lambda = 10$, and $g_s^* = 0.380$ for $\lambda = 50$; and of types (b) and (c): $g_s^* = 0.322$ for $\lambda = 10$, and $g_s = 0.285$ for $\lambda = 50$. All the calculated thresholds coincide perfectly with $g_s^{(n=2)}/k$.

Finally, we have tested robustness of the synchronization with respect to a mismatch in the synaptic strengths. We have simulated networks of 20 neurons for the local, intermediate and global cases, introducing a mismatch in the synaptic strengths around the average g_s. Perfect synchronization is no longer possible in these cases, due to the absence of the synchronization manifold, and there is always an error in the synchronization. However, for a given value of g_s this error falls rapidly and then remains constant when g_s is further increased. This point can be seen as the coupling threshold for the approximate synchronization. In all sim-

ulated cases this value is nearly identical to the synchronization threshold without mismatch as shown in Fig 4. The synchronization has been verified to be robust for mismatches in g_s of up to 5%.

The derivation of condition (25) mainly relies on two properties of the coupled system: (i) the spiking state, which is most resistant to synchronization, encircles the right branch of the fast nullcline $f(x)$, where the contribution of coupling is strong; (ii) the quiescent state, which is easy to synchronize, belongs to the left branch of $f(x)$. These properties are typical for square-wave and parabolic bursters, whose formation involves the two branches of $f(x)$. Consequently, the synchronization condition (25) is not restricted to the HR neuron, but is applicable to other Hodgkin-Huxley-type neurons, exhibiting square-wave and parabolic bursters. For example, two Sherman models displaying square-wave bursting for the standard parameters [20], synchronize at $g_{\rm s}^{(n=2)} = 0.25$ when synaptically coupled with $\Theta_{\rm s} = -40$, $V_s = -10$, and $\lambda = 50$. The synchronization thresholds in a larger network (9) of the Sherman models correspond to the values predicted by $g_{\rm s}^{(n=2)}/k$.

This completes our study of stable complete synchronization in the network (9) with any coupling configuration admitting synchronization. In the next section, we consider the existence and stability of synchronous clusters in the network (9).

4 Clusters of synchrony

4.1 Existence of synchronous clusters

Synchronous clusters exist if the graph vertices have a corresponding balanced coloring [43, 44, 45]. Every cluster of synchrony corresponds to a coloring of the graph vertices in which two vertices have the same color if and only if their states are equal (completely synchronized). Vertices colored in this way create a coloring map.

Definition 1. A coloring of the vertices is balanced, if each vertex of color i gets the same number of inputs from the vertices of color j, for all i and j.

That is, we color the vertices from the cluster decomposition V according to the following rule. We assign the same color to vertices (neurons) if their coordinates in the corresponding linear subspace $M(d)$ are equal. Coloring is balanced if all cells with the same color receive equal number of inputs from cells of a given color. The linear subspace $M(d)$ is flow-invariant if and only if the chosen coloring is balanced [43].

Definition 2. A minimal balanced coloring is a balanced coloring with the minimal number of colors.

Note that the above coloring differs from the classical definition used in graph theory. Indeed, graph theory defines a coloring of a graph as an assignment of colors to the vertices, one color to each vertex, so that adjacent vertices are assigned different colors. The minimum integer k for which a graph is k-colorable is called the

chromatic number [49]. However, our cluster partition and the associated balanced coloring allow two adjacent cells (vertices) to have the same color, provided that the two cells are input isomorphic [42], i.e. their dynamics are described by the same differential equations, up to a permutation of the variables [43].

In the following we use this concept to identify partitions with minimum number of clusters in networks (9) with regular and random structures. Finding a minimal balanced coloring in a given complex network is a non-trivial task. In this subsection, we propose a simple combinatorial algorithm that finds the minimal balanced coloring, and therefore identifies the largest synchronous clusters in the given (complex) network. In the next subsection, we address the stability of the clusters.

We shall first establish a few properties of balanced colorings before introducing an algorithm that allows finding a minimal balanced coloring.

Definition 3. A coloring C_2 is a refinement of a coloring C_1 if two vertices that have the same color in C_2 have the same color also in C_1.

Remark 6. a) We do not distinguish colorings where the subsets of vertices with the same color are the same, but the colors are different.
b) Any coloring is a refinement of the coloring where all vertices have the same color.
c) The coloring where all vertices have a different color is balanced and it is a refinement of any other coloring.
d) The set V_{1m} of vertices with color c_{1m} in C_1 is a union of sets V_{2p}, where V_{2p} is the set of all vertices with the same color c_{2p} in C_2.
e) If C_2 is a refinement of C_1, and C_1 is a refinement of C_2, the two colorings are the same (modulo the colors, cf. Remark 6a)).

We now introduce a special refinement in view of balancing.

Definition 4. The input driven refinement C_2 of a coloring C_1 is obtained as follows. Consider all vertices that have color c_m in C_1. Color them with the same color c_{mj} if they have the same number of inputs from all vertices of the same color $c_{m'}$ in C_1, for every color $c_{m'}$.

Property 4.1.
a) Either the input driven refinement C_2 of C_1 has more colors than C_1 or C_2 is equal to C_1 (modulo the colors) and balanced.
b) Suppose that a balanced coloring C_2 is a refinement of a (not necessarily balanced) coloring C_1. Let C_3 be the input driven refinement of C_1. Then C_2 is also a refinement of C_3.

Proof. Property 4.1a) follows immediately from Definition 4. For the proof of Property 4.1b) suppose that two vertices v and w have the same color in C_2. We have to show that they also have the same color in C_3. Since C_2 is a refinement of C_1, v and w also have the same color in C_1. Now consider the set V_{2p} that have the color c_{2p} in C_2. Again, they must also have the same color in C_1. Furthermore, since C_2 is a balanced coloring, the number of inputs from V_{2p} to v is the same as the number of inputs from V_{2p} to w. This is true for any color c_{2p} of C_2. Now consider the set

V_{1m} of vertices that have color c_{1m}. Then according to the above remark, V_{1m} is a union of sets V_{2p}. From each of the sets V_{2p} there is the same number of inputs to the vertices v and w and therefore there is also the same number of inputs from V_{1m} to v and w. As this holds for any color c_{1m}, by the construction of C_3, v and w must have the same color in C_3. □

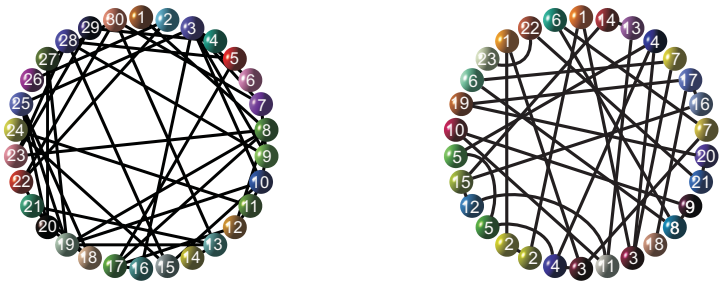

Fig. 6 Clusters of synchrony in random networks of 30 neurons. (Left): Network generated by randomly choosing a link between any two nodes with probability $p = 0.045$. There are 30 independent clusters, each represented by one distinct neuron. Neurons do not form clusters of synchrony due to the lack of symmetry. (Right): Random network with 23 clusters. Links are generated with uneven probabilities. Note clusters formed by vertices with the same index.

Property 4.1 and Remark 6a suggest the following algorithm to obtain a minimal balanced coloring:

Algorithm for finding synchronous clusters:

Initialization: Start with the coloring where all vertices are colored with the same color.

Repeat: Replace the current coloring with the input driven refinement of the current coloring until no new refinement is obtained.

The following property follows immediately from Property 4.1.

Property 4.2.

a) The algorithm stops in a finite number of steps. The maximum number of steps is the number of vertices in the graph.

b) The coloring, obtained when the algorithm stops, is balanced.

Corollary 4.1: Given a directed graph, the minimal balanced coloring is unique and it is obtained by the above algorithm.

Proof. According to Property 4.1b) any balanced coloring C_b is a refinement of all colorings obtained during the execution of the algorithm. It is in particular a refinement of the balanced coloring $C_{\min}$ obtained when the algorithm stops. Therefore, $C_{\min}$ is minimal. Furthermore, if there was another minimal balanced coloring C_m, it would also have to be a refinement of $C_{\min}$. But since C_m is minimal, it must be equal to $C_{\min}$ (modulo the colors). □

We have applied our combinatorial algorithm to a number of regular and random networks. Three of them are shown in Figs. 6 and 7. The application of our algorithm has shown that random networks generated with uniform probability per link appearance rarely have clusters of synchrony, whereas pseudorandom networks (cf. Fig. 6 (right)) may have a hidden subnetwork modular structure that yields clusters of synchrony.

The stability of clusters in networks of bursting neurons (9) depends on various factors, including the individual neuron dynamics and network topology. In the next section, we prove the stability of specific clusters of synchrony in networks (9). The stability conditions for irregular cluster configurations are often tedious and will be reported elsewhere.

4.2 Stability of clusters in multi-layer networks

We use the pyramidal-shape network of Fig. 7 as a representative example of multi-layer networks where the cells from each layer receive a common input from the same driving neurons. The network of Fig. 7 with uniform symmetrical connections has a four-color partition, corresponding to four clusters of synchrony that are defined by $M(4) = \{\xi_2(t) = \xi_3(t), \xi_4(t) = \xi_5(t) = \xi_6, \xi_7(t) = \xi_8(t) = \xi_9(t) = \xi_{10}(t)\}$, $\xi_i = (x_i, y_i, z_i)$.

In the following, we derive stability conditions for the four clusters in the network (2) with the above four-layer structure. The stability equations (2) for the transverse perturbations to the linear invariant manifold $M(4)$ take the form

$$\begin{aligned}
\dot{X}_{c2} &= (2ax_{c2} - 3x_{c2}^2)X_{c2} - Y_{c2} - Z_{c2} - g_s\left[\Gamma(x_{c1}) + 3\Gamma(x_{c3})\right]X_{c2} \\
\dot{Y}_{c2} &= 2(a+\alpha)x_{c2}X_{c2} - Y_{c2} \\
\dot{Z}_{c2} &= \mu(bX_{c2} - Z_{c2}) \\
\dot{X}_{c3} &= (2ax_{c3} - 3x_{c3}^2)X_{c3} - Y_{c3} - Z_{c3} - g_s\left[2\Gamma(x_{c2}) + 4\Gamma(x_{c4})\right]X_{c3} \\
\dot{Y}_{c3} &= 2(a+\alpha)x_{c3}X_{c3} - Y_{c3} \\
\dot{Z}_{c3} &= \mu(bX_{c3} - Z_{c3}) \\
\dot{X}_{c4} &= (2ax_{c4} - 3x_{c4}^2)X_{c4} - Y_{c4} - Z_{c4} - 3g_s\Gamma(x_{c3})X_{c4} \\
\dot{Y}_{c4} &= 2(a+\alpha)x_{c4}X_{c4} - Y_{c4} \\
\dot{Z}_{c4} &= \mu(bX_{c4} - Z_{c4})
\end{aligned} \tag{26}$$

Here, $\{X_{c2}, Y_{c2}, Z_{c2}\}$, $\{X_{c3}, Y_{c3}, Z_{c3}\}$ and $\{X_{c4}, Y_{c4}, Z_{c4}\}$ are infinitesimal differences between the coordinates of the neurons from clusters $\{C2 : \xi_2 = \xi_3\}$, $\{C3 : \xi_4 = \xi_5 = \xi_6\}$, and $\{C4 : \xi_7 = \xi_8 = \xi_9 = \xi_{10}\}$, respectively. The first cluster $C1$ is represented by one, unsynchronized neuron from layer 1. Technically, we should have considered the difference stability equations for any pair of neurons from the same cluster. However, due to the layer-structure of the network in which each neuron from a given cluster receives inputs from the same neurons, these stability equations are identical and can be replaced by a system of only three stability equations for each cluster. In (26), the variables (x_{ci}), $i = 1, .., 4$ are governed by the system (10) with

the number of inputs $k_i = 2,4,6,3$, respectively. System (26) is an analog of the

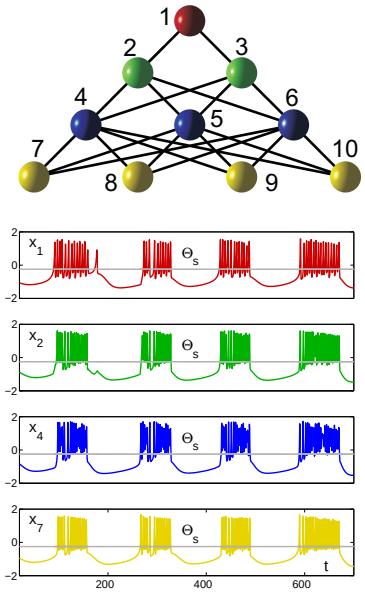

Fig. 7 Multi-layer network with symmetrical connections (top). Cells with the same color belong to the same cluster. Time-series of four synchronous clusters. Note that the time-series are synchronized at the level of bursts but there is spike asynchrony between the clusters. Neurons within the clusters are synchronized completely.

Master Stability (MS) function [6] for the stability of the cluster synchronization. MS functions of this kind are usually analyzed numerically. Completely rigorous derivation of an upper bound for the coupling threshold sufficient for cluster synchronization is complicated as the X stability equation of each cluster is also driven by neurons from other clusters. To get around this difficulty, we make the following simplification. Numerical simulations show that when cluster synchronization takes place and neurons split into clusters of perfect synchrony, all neurons of the network also become synchronized at the level of bursts but there is no spike synchrony among the clusters (see Fig. 7). As a result, the network behavior possesses two distinct mesoscopic and macroscopic properties: synchronization within the clusters representing the mesoscale and burst synchronization of the entire network at the macroscale. Burst synchronization implies that all the neurons start and cease bursting at the same time instant. Consequently, the variables defining the four clusters of perfect synchrony: x_{c1}, x_{c2}, x_{c3}, and x_{c4} cannot be equal. However, the corresponding synaptic functions $\Gamma(x_{c1})$, $\Gamma(x_{c2})$, $\Gamma(x_{c3})$, and $\Gamma(x_{c4})$ become approximatively equal as the neurons states cross the synaptic threshold Θ_s and therefore activate the synaptic functions $\Gamma(x_{ci})$ at approximatively same times. Using this approximation that $\Gamma(x_{c1}) = \Gamma(x_{c2}) = \Gamma(x_{c3}) = \Gamma(x_{c4})$, we can transform the stability equation

(26) as follows:

$$\begin{aligned}
\dot{X}_{c2} &= (2ax_{c2} - 3x_{c2}^2)X_{c2} - Y_{c2} - Z_{c2} - 4g_s\Gamma(x_{c2})X_{c2} \\
\dot{Y}_{c2} &= 2(a+\alpha)x_{c2}X_{c2} - Y_{c2} \\
\dot{Z}_{c2} &= \mu(bX_{c2} - Z_{c2}) \\
\dot{X}_{c3} &= (2ax_{c3} - 3x_{c3}^2)X_{c3} - Y_{c3} - Z_{c3} - 6g_s\Gamma(x_{c3})X_{c3} \\
\dot{Y}_{c3} &= 2(a+\alpha)x_{c3}X_{c3} - Y_{c3} \\
\dot{Z}_{c3} &= \mu(bX_{c3} - Z_{c3}) \\
\dot{X}_{c4} &= (2ax_{c4} - 3x_{c4}^2)X_{c4} - Y_{c4} - Z_{c4} - 3g_s\Gamma(x_{c4})X_{c4} \\
\dot{Y}_{c4} &= 2(a+\alpha)x_{c4}X_{c4} - Y_{c4} \\
\dot{Z}_{c4} &= \mu(bX_{c4} - Z_{c4})
\end{aligned} \tag{27}$$

Note that three subsystems for the stability of clusters $C2$, $C3$, and $C4$ are independent. The new stability system (27) is stabilized as long as its weakest subsystem, corresponding to the cluster $C4$ that receives the fewest number of inputs, becomes stable. This statement can be verified by constructing a Lyapunov function similar to the function (17), written for all nine coordinates of the system (27) and showing that its derivative splits into three independent quadratic forms. Each quadratic form corresponds to the stability of each cluster, and the negativeness of the form corresponding to the cluster $C4$ with the fewest number of inputs ensures the negativeness of the other two quadratic forms. For the sake of brevity, we have omitted this proof. In short, the linear invariant manifold $M(4)$ defining the cluster partition is locally stable as long as the origin of the following system is stable

$$\begin{aligned}
\dot{X}_{c4} &= (2ax_{c4} - 3x_{c4}^2)X_{c4} - Y_{c4} - Z_{c4} - 3g_s\Gamma(x_{c4})X_{c4} \\
\dot{Y}_{c4} &= 2(a+\alpha)x_{c4}X_{c4} - Y_{c4} \\
\dot{Z}_{c4} &= \mu(bX_{c4} - Z_{c4}).
\end{aligned} \tag{28}$$

Statement 2. *Under the numerically validated approximation that $\Gamma(x_{c1}) = \Gamma(x_{c2}) = \Gamma(x_{c3}) = \Gamma(x_{c4})$ in the regime of cluster synchronization, an upper bound for the coupling threshold that guarantees local stability of cluster synchronization in the network (2) with the structure of Fig. 7 becomes*

$$g_s^* = \max\{2D_1/3, 2D_2/3, D_3^{\mathrm{cl}}\}, \text{ where} \tag{29}$$

constants D_1 and D_2 are given in the condition (15) of Theorem 1 with $k = 1$. Here, the new constant $D_3^{\mathrm{cl}} = \frac{p}{3\beta}(1 + e^{-\lambda(b-\Theta_s)})$, and parameters p, b, and β are given in (15).

Proof. The stability system (28) is similar to the variational equations (13)-(14) for the stability of complete synchronization in the simplest globally coupled two-neuron network (2) with $k = 1$. Use the Lyapunov function (17) and follow the steps of the proof of Theorem 1, replacing the function $\Omega(x)$ with $3g_s\Gamma(x)$. Note that the lowest bound of $3g_s\Gamma(x)$ in the region $x \geq \Theta_s$ is $3/2$. Therefore, Conditions I and II (Part I) of the above proof yield the bounds $2D_1/3$ and $2D_2/3$. The stability condition (20) for the part of the synchronous trajectory $x_{c4} < \Theta_s$ turns into $g_s = D_3^{\mathrm{cl}} = \frac{p}{3\beta}(1 + e^{-\lambda(b-\Theta_s)})$. □

Note that the obtained bound (29) is not completely rigorous as opposed to the rigorous bounds for complete synchronization derived in Theorems 1 and 2. The above approximation only holds to a certain degree of precision and comes from numerical simulations. However, it clearly shows that the stability of cluster synchronization in the multi-layer network (2) is determined by the stability of the cluster with the smallest number of inputs. In our case, this is cluster $C4$, representing layer 4 of the network in which the neurons receive three inputs.

5 Conclusions

Networks of synaptically coupled neurons have very different synchronization properties from linearly (gap-junction) coupled neurons. In the case of identical neurons with identical excitatory coupling functions and coupling constants, complete synchronization is only possible when each neuron receives the same number of inputs from other neurons [27]. In this case, we have showen that the single condition (25) ensures the onset of complete synchronization in networks of synaptically coupled bursting neurons (9) with any coupling topology in which each neuron receives signals from k others. The synchronization condition depends on the number of inputs k and *not* on the connectivity matrix. This condition carries over to burst synchronization when the neurons are non-identical and the synaptic connections are heterogeneous, provided that the total input, each neuron receives, is roughly the same. Burst synchronization occurs when the envelopes of the spikes synchronize, but there is no synchrony among the spikes.

The equal k constraint is often invalid for biologically relevant networks with a complex structure where the number of inputs is not necessarily constant, but if k is uniform for a group of neurons, synchronization within this cluster of neurons can occur. The possible cluster decompositions of the network can be identified from the network topology alone through a so-called balanced coloring of the vertices [43, 44, 45]. Among the balanced colorings there is a unique coloring that uses the minimal number of colors, corresponding to a cluster decomposition with the smallest number of clusters, and therefore to the largest clusters. With sufficiently strong coupling, the neurons within these clusters synchronize. We have given a simple algorithm that finds this cluster decomposition from the network topology. Networks with a certain degree of internal symmetries are likely to have cluster decompositions with relatively large clusters, leading potentially to synchronization at mesoscale, whereas random graphs rarely admit clusters composed of more than two or three neurons. We have also addressed the important question of the (local) asymptotic stability of cluster synchronization. This property depends not only on the network topology, but also on the neuron models themselves. We have concentrated on the Hindmarsh-Rose model in the range of parameters where square-wave bursting takes place. We have given an explicit rigorous threshold for the coupling strength that guarantees the asymptotic stability of local synchronization in globally and densely coupled neurons. We have then used a similar stability argument to es-

tablish thresholds for the stability of cluster synchronization in well-structured networks where each cluster receives the same inputs from other neurons. Our analysis demonstrates that the stability of the cluster synchronization in the entire network is determined by the stability of the cluster composed of two or more neurons with the smallest number of inputs.

The synaptic strengths in biologically relevant networks with a complex structure can change as a result of pre- and postsynaptic neuron activity. This may result in temporally approximate cluster synchronization when the total input to groups of neurons becomes color balanced only for a specific interval of time. The proposed algorithm promises to allow finding temporal clusters of synchrony in networks with time-varying synapses. Its extension to adaptive networks with the ability to privilege clusters of synchrony is a subject of separate study.

Acknowledgements This work was supported by the National Science Foundation under Grant DMS-1009744, the GSU Brains and Behavior program, and RFFI Grants N 2100-065268 and N 09-01-00498-a (to I.B.).

References

1. Sporns, O.: Scholarpedia **2**(10), 4695 (2007).
2. Watts, D.J. and Strogatz, S.H.: Nature **393**, 440 (1998).
3. Strogatz, S.H.: Nature **410**, 268 (2001).
4. Afraimovich, V.S., Verichev, N.N., and Rabinovich, M.I.: Izv. Vuzov. Radiofiz. **29**, 795 (1986).
5. Pecora, L.M. and Carroll, T.L.: Phys. Rev. Lett. **64**, 821 (1990).
6. Pecora, L.M. and Carroll, T.L: Phys. Rev. Lett. **80**, 2109 (1998).
7. Barahona, M. and Pecora, L.M.: Phys. Rev. Lett. **89**, 054101 (2002).
8. Nishikawa, T, Motter, A.E., Lai, Y.-C., and Hoppensteadt, F.C.: Phys. Rev. Lett. **91**, 014101 (2003).
9. Belykh, V.N., Belykh, I.V., and Hasler, M.: Physica (Amsterdam) **195D**, 159 (2004).
10. Almendral, J., Leyva, I., Daqing, L., Sendina-Nadal, I., Shlomo, H., and Boccaletti, S.: Phys. Rev. E **82**, 016115 (2010).
11. Rodriguez-Caso, C., Corominas-Murtra, B., Sole, R.V.: Molecular Biosystems **5**, 1617 (2009).
12. Newman, M.E.J.: Proc. Natl. Acad. Sci. USA **103** (23), 8577 (2006).
13. Boccaletti, S., Latora, V., Moreno, Y., Chavez, M., Hwang, D.-U.: Physics Reports **424**, 175 (2006).
14. Afraimovich, V.S. and Bunimovich, L.A.: Nonlinearity **20**, 1761 (2007).
15. Afraimovich, V.S., Zhigulin, V.P., and Rabinovich, M.I.: Chaos **14**(4), 1123 (2004).
16. Afraimovich, V.S., Yong, T., Muezzinoglu M.K., and Rabinovich, M.I.: Bull Math Biol. **73**(2), 266 (2011).
17. Gray, C. M. and Singer, W.: Proc. Natl. Acad. Sci. USA **86**, 1698 (1989); Bazhenov, M., Stopfer, M., Rabinovich, M.I., Huerta, R., Abarbanel, H.D.I., Sejnowski, T.J., and Laurent, G.: Neuron **30**, 553 (2001); Mehta, M. R., Lee, A. K. , and Wilson, M. A.: Nature **417**, 741 (2002).
18. Ermentrout, G. B. and Kopell, N.: SIAM J. Appl. Math., **46** 233 (1986).
19. Sherman, A. and Rinzel, J.: Proc. Natl. Acad. Sci. USA **89**, 2471 (1994).
20. Sherman, A., Bull. Math. Biol. **56**, 811 (1994).
21. Terman, D. and Wang, D.: Physica (Amsterdam) **81D**, 148 (1995).
22. Rabinovich, M.I., Torres, J.J., Varona, P., Huerta, R., and Weidman, P.: Phys. Rev E **60**, R1130-R1133 (1999).

23. Izhikevich, E.M.: SIAM Rev. **43**, 315 (2001).
24. Rubin, J. and Terman, D.: SIAM J. Appl. Dyn. Sys. **1**, 146 (2002).
25. Dhamala, M., Jirsa, V.K., and Ding, M.: Phys. Rev. Lett. **92**, 074104 (2004).
26. de Vries, G. and Sherman, A.: in S. Coombes and P.C. Bressloff (Editors), *Bursting: The Genesis of Rhythm in the Nervous System* (World Scientific Publishing, London, 2005) pp. 243-272.
27. Belykh, I., de Lange, E., Hasler, M.: Phys. Rev. Lett. **94**, 188101 (2005).
28. Belykh, I. and Shilnikov, A.: Phys. Rev. Lett. **101**, 078102 (2008).
29. Shilnikov, A., Gordon, R., and Belykh, I.: Chaos **18**, 037120 (2008).
30. Jalil, S., Belykh, I., and Shilnikov, A.: Phys. Rev. E **81**, R045201 (20010).
31. Rinzel, J.: Lecture Notes in Biomathematics, Vol. 71 (Springer-Verlag, Berlin, 1987), pp. 251-291.
32. Terman, D.: SIAM J. Appl. Math, **51**, 1418 (1991).
33. Bertram, R., Butte, M.J., Kiemel, T., and Sherman, A.: Bull. Math. Biol. **57**, 143 (1995).
34. Belykh, V.N, Belykh, I.V, Colding-Joergensen, M., and Mosekilde, E.: Europ. Phys. J. E **3**, 205 (2000).
35. Izhikevich, E.M.: Int. J. Bifurc. Chaos **10**, 1171 (2000).
36. Shilnikov, A. and Cymbalyuk, G.: Phys. Rev. Lett. **94**, 048101 (2005).
37. Shilnikov, A., Calabrese, R., and Cymbalyuk, G.: Phys. Rev. E **71**, 056214 (2005).
38. Frohlich, F. and Bazhenov, M.: Phys. Rev. E **74**, 031922 (2006).
39. Pogromsky, A.Yu. and Nijmeijer, H.: IEEE Trans. Circuits Syst., I: Fundam. Theory Appl. **48**, 152 (2001).
40. Belykh, V., Belykh, I., and Hasler, M.: Phys. Rev. E **62**, 6332 (2000).
41. Belykh, I., Belykh, V., Nevidin, K., and Hasler, M.: Chaos **13**, 165 (2003).
42. Stewart, I., Golubitsky, M., and Pivato, M.: SIAM J. Appl. Dynam. Sys. **2**, 609 (2003).
43. Golubitsky, M., Stewart, I., Torok, A.: SIAM J. Appl. Dynam. Sys. **4**, 78 (2005).
44. Golubitsky, M., Stewart, I.: Bull. Amer. Math. Soc. **43**, 305 (2006).
45. Wang, Y. and Golubitsky, M.: Nonlinearity, **18**, 631 (2005).
46. Belykh, I. and Hasler, M.: Chaos **21**, 016106 (2011).
47. Hindmarsh, J.L. and Rose, M.: Proc. R. Soc. London, Ser. B **221**, 87 (1984).
48. Wang, X.-J.: Physica (Amsterdam) **62D**, 263 (1993).
49. Bollobas, B.: Modern Graph Theory, (Springer-Verlag, New York, 1998).
50. Shilnikov, A.L. and Kolomiets, M.L.: Int. J. Bifurcation Chaos **18**, (8) 1 (2008).
51. Storace, M., Linaro, D., and de Lange, E: Chaos **18**, 033128 (2008).
52. Bautin, N.N.: *Behavior of Dynamical Systems Near the Boundary of Stability* (Nauka Publ. House, Moscow, 1984).
53. Somers, D and Kopell, N.: Biol. Cybern. **68** 393 (1993).
54. Wang, X.F. and Chen, G.: IEEE Trans. Circuits Syst., I: Fundam. Theory Appl. **49**, 54 (2002).